MULTILAYER GRAPHENE

I. SCALES OF THE HAMILTONIAN

We set $\hbar = 1$ throughout all the text. The UV cutoff $\mathcal{K}$ of the system, fixed by the lattice parameter $2\pi/\mathcal{K}$, provides us a natural scale to measure the momenta, such that any momentum index $\mathbf{k}$ is normalized by $\mathcal{K}$. In this way, we get the kinetic non-interacting Hamiltonian

$$H_{\text{kin}} = E_{\text{UV}} \sum_{\mathbf{k}\sigma\sigma'} \left(\frac{|\mathbf{k}|}{\mathcal{K}}\right)^m \psi^\dagger_{\mathbf{k},\sigma} \left(\hat{\mathbf{k}}_m \cdot \boldsymbol{\sigma}_{\sigma\sigma'}\right) \psi_{\mathbf{k},\sigma'}, \quad (1)$$

where $[\hat{\mathbf{k}}_m] = \big(\cos(m\phi_m)\ \sin(m\phi_m)\big)$ and E_{UV} is the numerical value of the kinetic term evaluated at $\mathcal{K}$, and whose shape depends on m:

- $m = 1$: $E_{\text{UV}} = v\mathcal{K}$, where v is the Fermi velocity of the Dirac fermions.
- $m = 2$: $E_{\text{UV}} = \mathcal{K}^2/2m_e$, where m_e is the effective mass of the electron.

The potential is given by

$$V_{\mathbf{r}} = V_0 e^{-r^2/2a^2} \quad (2)$$

with V_0 the intensity of the Gaussian potential and a the spreading in the real space. Its Fourier transform is

$$V_{\mathbf{k}} = 2\pi a^2 V_0 e^{-\frac{a^2k^2}{2}} = \frac{E_{\text{UV}}}{\mathcal{K}^2}\left[\frac{2\pi(a\mathcal{K})^2 V_0}{E_{\text{UV}}} e^{-\frac{(a\mathcal{K})^2}{2}\left(\frac{k}{\mathcal{K}}\right)^2}\right],$$

$$V_{\mathbf{k}} = \frac{E_{\text{UV}}}{\mathcal{K}^2}\left(g_0 e^{-\frac{a^2_{\mathcal{K}}}{2}\left(\frac{k}{\mathcal{K}}\right)^2}\right), \quad (3)$$

where $k = |\mathbf{k}|$. It is assumed that $a > 2\pi/\mathcal{K}$, i.e., the spreading of the Gaussian should be larger than the lattice parameter $2\pi/\mathcal{K}$. The additional two nondimensional parameters are:

- Reciprocal spreading $a_{\mathcal{K}} = a\mathcal{K}$: Determines how concentrated is the potential in the reciprocal space. $a_{\mathcal{K}}$ is constrained to be larger than one.
- Coupling constant $g_{\mathcal{K}} = 2\pi a^2_{\mathcal{K}} V_0/E_{\text{UV}}$: Relates the intensity of the Gaussian potential in the reciprocal space with E_{UV}, the kinetic energy at the UV cutoff.

Lastly, the interaction Hamiltonian can be expressed as

$$H_{\text{int}} = \frac{1}{2A}\sum_{\mathbf{k}\mathbf{k}'}\sum_{\sigma\sigma'} V_{\mathbf{q}} \psi^\dagger_{\mathbf{k}'+\mathbf{q},\sigma'} \psi^\dagger_{\mathbf{k}-\mathbf{q},\sigma} \psi_{\mathbf{k},\sigma} \psi_{\mathbf{k}',\sigma'} \quad (4)$$

$$= \frac{E_{\text{UV}}}{2A\mathcal{K}^2}\sum_{\mathbf{k}\mathbf{k}'}\sum_{\sigma\sigma'} g_{\mathcal{K}} e^{-\frac{a^2_{\mathcal{K}}}{2}\left(\frac{k}{\mathcal{K}}\right)^2} \psi^\dagger_{\mathbf{k}'+\mathbf{q},\sigma'} \psi^\dagger_{\mathbf{k}-\mathbf{q},\sigma} \psi_{\mathbf{k},\sigma} \psi_{\mathbf{k}',\sigma'}.$$

where A is the total area of the system.

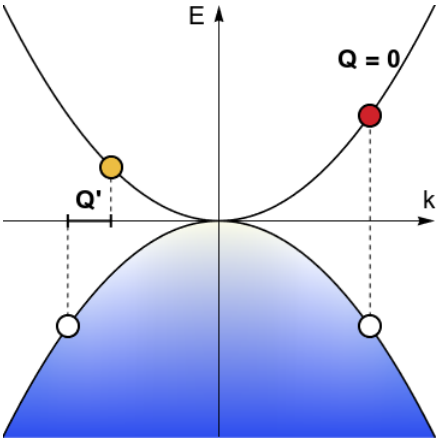

FIG. 1. $\mathbf{Q} = 0$ and $\mathbf{Q} \neq 0$ excitations on the parabolic bands.

II. RESTRICTED HILBERT SPACE FOR $\mathbf{Q} = 0$ EXCITONS AND PSEUDOSPIN BASIS

The optical relevant excitations of the system correspond to the $\mathbf{Q} = 0$ excitons, as shown in Fig. 1. These ones do not modify the momentum label of the electron when it jumps from the valence to the conduction band, and consequently, any interaction between a pair excitons at momenta $\mathbf{k}_1$ and $\mathbf{k}_2$ should only interchange their momentum labels. In other words, by having into account only $\mathbf{Q} = 0$ excitations, the Hilbert space of the system results restricted onto the singly-occupied sites in the momentum lattice. A good operator to describe the singly-occupied constrain is

$$s^\mu_{\mathbf{k}} = \sum_{\sigma\sigma'} \psi^\dagger_{\mathbf{k},\sigma} \sigma^\mu_{\sigma\sigma'} \psi_{\mathbf{k},\sigma'}. \quad (5)$$

where $\sigma^\mu_{\sigma,\sigma'}$ is the component $\sigma\sigma'$ of the matrix σ^μ, given by the generators ot the SU(2) Lie algebra, i.e., the Pauli matrices and the identity

$$\sigma^0 = \begin{pmatrix} 1 & 0 \\ 0 & 1 \end{pmatrix}, \quad \sigma^1 = \begin{pmatrix} 0 & 1 \\ 1 & 0 \end{pmatrix}, \quad \sigma^2 = \begin{pmatrix} 0 & -i \\ i & 0 \end{pmatrix}, \quad \sigma^3 = \begin{pmatrix} 1 & 0 \\ 0 & -1 \end{pmatrix}, \quad (6)$$

The matrix σ^0 is useful to express the singly-occupied condition as the constrain

$$s^0_{\mathbf{k}} = \sum_{\sigma\sigma'} \psi^\dagger_{\mathbf{k},\sigma} \sigma^0_{\sigma\sigma'} \psi_{\mathbf{k},\sigma'} = \sum_{\sigma\sigma'} \psi^\dagger_{\mathbf{k},\sigma} \delta_{\sigma\sigma'} \psi_{\mathbf{k},\sigma'} = \sum_{\sigma\sigma'} \psi^\dagger_{\mathbf{k},\sigma} \psi_{\mathbf{k},\sigma} = \sum_{\sigma} n_{\mathbf{k},\sigma} = 1. \quad (7)$$

.

The following steps show how the four-fermion term in the interacion Hamiltonian can be expressed under the singly-occupied constrain. The completeness relation of the Pauli matrices

$$\sum_{\mu=0}^{3} \sigma^\mu_{\sigma\sigma'} \sigma^\mu_{\tau\tau'} = 2\delta_{\sigma\tau'}\delta_{\sigma'\tau}, \quad (8)$$

and the trace of Pauli matrices bilinears

$$\mathrm{tr}\left(\sigma^{\mu}\sigma^{\mu'}\right)=\sum_{\tau,\tau'}\sigma^{\mu}_{\tau\tau'}\sigma^{\mu'}_{\tau'\tau}=2\delta^{\mu\mu'}, \tag{9}$$

are useful to find the inverse relation between fermion bilinears and Pauli matrices

$$\begin{aligned}\sum_{\mu=0}^{3}\sigma^{\mu}_{\tau\tau'}s^{\mu}_{\mathbf{k}}&=\sum_{\mu=0}^{3}\sum_{\sigma\sigma'}\psi^{\dagger}_{\mathbf{k},\sigma}\sigma^{\mu}_{\sigma\sigma'}\sigma^{\mu}_{\tau,\tau'}\psi_{\mathbf{k},\sigma'}\\&=2\sum_{\sigma\sigma'}\psi^{\dagger}_{\mathbf{k},\sigma}\delta_{\sigma\tau'}\delta_{\sigma'\tau}\psi_{\mathbf{k},\sigma'}\\&=2\psi^{\dagger}_{\mathbf{k},\tau'}\psi_{\mathbf{k},\tau}.\end{aligned} \tag{10}$$

In this way, the fermion bilinears can then be expanded in terms of the generators of the Lie algebra of the group SU(2)

$$\psi^{\dagger}_{\mathbf{k},\tau'}\psi_{\mathbf{k},\tau}=\frac{1}{2}\sum_{\mu=0}^{3}s^{\mu}_{\mathbf{k}}\sigma^{\mu}_{\tau\tau'}, \tag{11}$$

The Eq. (11) is then useful to express the four-fermion term of the interaction Hamiltonian after some anticommutations to match fermion operators that share the same momentum label, such as follows

$$\begin{aligned}&\sum_{\tau,\tau'}\left(\psi^{\dagger}_{\mathbf{k},\tau}\psi_{\mathbf{k},\tau'}\right)\left(\psi^{\dagger}_{\mathbf{k}',\sigma}\psi_{\mathbf{k}',\sigma'}\right)=\\&=\sum_{\tau,\tau'}\left(\frac{1}{2}\sum_{\mu=0}^{3}\sigma^{\mu}_{\tau'\tau}s^{\mu}_{\mathbf{k}}\right)\left(\frac{1}{2}\sum_{\mu'=0}^{3}\sigma^{\mu'}_{\tau\tau'}s^{\mu'}_{\mathbf{k}'}\right)\\&=\frac{1}{4}\sum_{\mu,\mu'}s^{\mu}_{\mathbf{k}}s^{\mu'}_{\mathbf{k}'}\sum_{\tau,\tau'}\sigma^{\mu}_{\tau'\tau}\sigma^{\mu'}_{\tau\tau'}\\&=\frac{1}{4}\sum_{\mu,\mu'}s^{\mu}_{\mathbf{k}}s^{\mu'}_{\mathbf{k}'}\mathrm{tr}\left(\sigma^{\mu}\sigma^{\mu'}\right)\\&=\frac{1}{2}\sum_{\mu,\mu'}s^{\mu}_{\mathbf{k}}s^{\mu'}_{\mathbf{k}'}\delta^{\mu\mu'}=\frac{1}{2}\sum_{\mu,\mu'}s^{\mu}_{\mathbf{k}}s^{\mu}_{\mathbf{k}'}=\frac{1+\mathbf{s}_{\mathbf{k}}\cdot\mathbf{s}_{\mathbf{k}'}}{2}\end{aligned} \tag{12}$$

Consequently, the original fermion Hamiltonian projected onto the singly-occupied is expressed as

$$\begin{aligned}&\mathcal{P}H\mathcal{P}=\\&E_{\mathrm{UV}}\sum_{\mathbf{k}}\left(\frac{|\mathbf{k}|}{\mathcal{K}}\right)^{m}\hat{\mathbf{k}}_{m}\cdot\mathbf{s}_{\mathbf{k}}-\sum_{\mathbf{k}_1\neq\mathbf{k}_2}\frac{V_{\mathbf{k}_1-\mathbf{k}_2}}{4A}\mathbf{s}_{\mathbf{k}_1}\cdot\mathbf{s}_{\mathbf{k}_2},\end{aligned} \tag{13}$$

where the first term represents a m-folded spin vortex (see Fig. 2) and the second term is an effective ferromagnetic exchange.

III. EXPANSION ABOUT THE NON-INTERACTING GROUND STATE

A. Band basis and interaction matrix

In this section, we provide details of the derivation of Eqs. (27) to (29) starting from Eq. (1). We begin

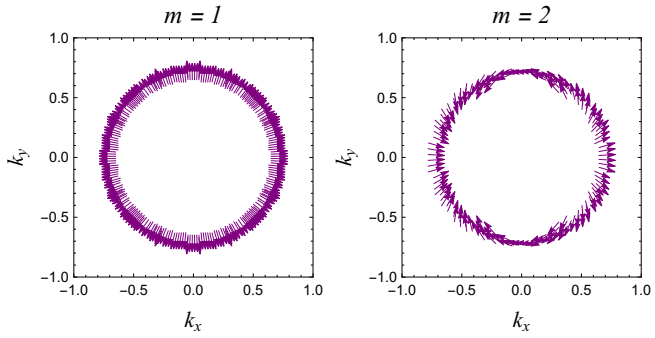

FIG. 2. Polar distribution of the vector $[\hat{\mathbf{k}}_m] = \big(\cos(m\phi_m)\ \sin(m\phi_m)\big)$ used to describe the classical ground state of the system.

describing the transfomation from pseudo-spin basis onto band basis. In the band basis $s=\{+,-\}$ the kinetic term is:

$$\begin{aligned}&\psi^{\dagger}_{\mathbf{k}\sigma}\left(\hat{\mathbf{k}}_m\cdot\boldsymbol{\sigma}_{\sigma\sigma'}\right)\psi_{\mathbf{k}\sigma'}=\\&\quad=e^{-im\phi}\psi^{\dagger}_{\mathbf{k}\uparrow}\psi_{\mathbf{k}\downarrow}+e^{+im\phi}\psi^{\dagger}_{\mathbf{k}\downarrow}\psi_{\mathbf{k}\uparrow}.\end{aligned} \tag{14}$$

Band and pseudospin basis are related by:

$$\begin{aligned}\psi_{\mathbf{k}\sigma}&=\sum_{s}\langle\sigma|\mathbf{k}s\rangle\,\psi_{\mathbf{k}s},\\\begin{pmatrix}\psi_{\mathbf{k}\uparrow}\\\psi_{\mathbf{k}\downarrow}\end{pmatrix}&=\frac{1}{\sqrt{2}}\begin{pmatrix}e^{-im\phi/2}&e^{-im\phi/2}\\e^{+im\phi/2}&-e^{+im\phi/2}\end{pmatrix}\begin{pmatrix}\psi_{\mathbf{k}+}\\\psi_{\mathbf{k}-}\end{pmatrix}.\end{aligned} \tag{15}$$

Fermion bilinears transform as

$$\sum_{\sigma}\psi^{\dagger}_{\mathbf{k}_1\sigma}\psi_{\mathbf{k}_2\sigma}=\psi^{\dagger}_{\mathbf{k}_1 s_1}\sum_{s_1 s_2}\langle\mathbf{k}_1 s_1|\mathbf{k}_2 s_2\rangle\,\psi^{\dagger}_{\mathbf{k}_1 s_1}\psi_{\mathbf{k}_2 s_2}, \tag{16}$$

where

$$\langle\mathbf{k}_1 s_1|\mathbf{k}_2 s_2\rangle=\begin{pmatrix}\cos m\phi_{12}/2&i\sin m\phi_{12}/2\\i\sin m\phi_{12}/2&\cos m\phi_{12}/2\end{pmatrix}, \tag{17}$$

where ϕ_i is the polar angle of $\mathbf{k}_i$, and $\phi_{12}=\phi_1-\phi_2$. Therefore, the Hamiltonian in Eq. (1) of the Main text in the band basis is expressed as follows:

$$\begin{aligned}\mathcal{P}H\mathcal{P}&=\sum_{\mathbf{k}}E^{m}_{\mathbf{k}}\left(\psi^{\dagger}_{\mathbf{k}+}\psi_{\mathbf{k}+}-\psi^{\dagger}_{\mathbf{k}-}\psi_{\mathbf{k}-}\right)\\&-\sum_{\mathbf{k}_1\neq\mathbf{k}_2}\sum_{s_1 s_2}(T^{m}_{\mathbf{k}_1\mathbf{k}_2})^{s_1 s_2}\psi^{\dagger}_{\mathbf{k}_1 s_1}\psi_{\mathbf{k}_1\bar{s}_1}\psi^{\dagger}_{\mathbf{k}_2\bar{s}_2}\psi_{\mathbf{k}_2 s_2},\end{aligned} \tag{18}$$

where $E^{m}_{\mathbf{k}}=E_{\mathrm{UV}}(|\mathbf{k}|/\mathcal{K})^{m}+\Sigma^{m}_{\mathbf{k}}$ is the effective dispersion relation of the electrons, in which $\Sigma^{m}_{\mathbf{k}}$ is the self-energy

$$\Sigma^{m}_{\mathbf{k}}=\frac{1}{2A}\sum_{\mathbf{p}}V_{\mathbf{k}-\mathbf{p}}\cos(m\phi_{\mathbf{kp}}). \tag{19}$$

and $(T^{m})^{s_1 s_2}_{\mathbf{k}_1\mathbf{k}_2}$ is the interaction matrix in the band basis, given by:

$$T^{m}_{\mathbf{k}_1\mathbf{k}_2}=\frac{V_{\mathbf{k_1}-\mathbf{k_2}}}{4A}\begin{pmatrix}1+\cos(m\phi_{12})&1-\cos(m\phi_{12})\\1-\cos(m\phi_{12})&1+\cos(m\phi_{12})\end{pmatrix}. \tag{20}$$

B. Holstein-Primakoff expansion

We select the following spin basis

$$\mathbf{s_k} = -s^z_{\mathbf{k}}\hat{\mathbf{k}}_m + s^x_{\mathbf{k}}\hat{\mathbf{z}} + s^y_{\mathbf{k}}\hat{\boldsymbol{\phi}}_m, \tag{21}$$

which diagonalizes the kinetic term, and where $\hat{\mathbf{z}}$ is the normal axis to the layer and $\hat{\boldsymbol{\phi}}_m = \hat{\mathbf{z}} \times \hat{\mathbf{k}}_m = \big(-\sin(m\phi_m)\ \cos(m\phi_m)\big)$, and the exchange term is expanded as

$$\begin{aligned}
&\hat{\mathbf{s}}_{\mathbf{k}} \cdot\ \hat{\mathbf{s}}_{\mathbf{k}'} \\
&= \left(-\hat{s}^z_{\mathbf{k}_1}\hat{\mathbf{k}} + \hat{s}^x_{\mathbf{k}}\hat{\mathbf{z}} + \hat{s}^y_{\mathbf{k}}\hat{\boldsymbol{\varphi}}\right) \cdot \left(-\hat{s}^z_{\mathbf{k}'}\hat{\mathbf{k}}' + \hat{s}^x_{\mathbf{k}'}\hat{\mathbf{z}} + \hat{s}^y_{\mathbf{k}'}\hat{\boldsymbol{\varphi}}'\right) \\
&= (\hat{s}^z_{\mathbf{k}}\hat{s}^z_{\mathbf{k}'} + \hat{s}^y_{\mathbf{k}}\hat{s}^y_{\mathbf{k}'})\cos\phi_{\mathbf{kk}'} + \hat{s}^x_{\mathbf{k}}\hat{s}^x_{\mathbf{k}'} \\
&+\ (\hat{s}^y_{\mathbf{k}}\hat{s}^z_{\mathbf{k}'} - \hat{s}^z_{\mathbf{k}}\hat{s}^y_{\mathbf{k}'})\sin\phi_{\mathbf{kk}'}
\end{aligned} \tag{22}$$

with $\cos\phi_{\mathbf{kk}'} = \hat{\mathbf{k}}\cdot\hat{\mathbf{k}}' = \hat{\boldsymbol{\varphi}}\cdot\hat{\boldsymbol{\varphi}}'$. On this basis, the Hamiltonian can be expanded in a bosonic representation by means of the Holstein-Primakoff (HP) transformations ($S = 1/2$):

$$\begin{aligned}
s^z_{\mathbf{k}} &= 2\left(S - b^\dagger_{\mathbf{k}}b_{\mathbf{k}}\right) = 1 - 2b^\dagger_{\mathbf{k}}b_{\mathbf{k}}, \\
s^x_{\mathbf{k}} &\approx \sqrt{2S}\left(b_{\mathbf{k}} + b^\dagger_{\mathbf{k}}\right) = b_{\mathbf{k}} + b^\dagger_{\mathbf{k}}, \\
is^y_{\mathbf{k}} &\approx \sqrt{2S}\left(b_{\mathbf{k}} - b^\dagger_{\mathbf{k}}\right) = b_{\mathbf{k}} - b^\dagger_{\mathbf{k}}.
\end{aligned} \tag{23}$$

The term corresponding to the exchange coupling in Eq. (13) can be transformed into pairing and hopping terms of bosons up to bilinears:

$$\begin{aligned}
\mathbf{s_k}\cdot\mathbf{s}_{\mathbf{k}'} \approx &\left(1 + b^\dagger_{\mathbf{k}}b_{\mathbf{k}} + b^\dagger_{\mathbf{k}'}b_{\mathbf{k}'}\right)\cos\phi_{\mathbf{kk}'} \\
&+ \left(b^\dagger_{\mathbf{k}}b_{\mathbf{k}'} + b_{\mathbf{k}}b^\dagger_{\mathbf{k}'}\right)(1 + \cos\phi_{\mathbf{kk}'}) \\
&+ \left(b^\dagger_{\mathbf{k}}b^\dagger_{\mathbf{k}'} + b_{\mathbf{k}}b_{\mathbf{k}'}\right)(1 - \cos\phi_{\mathbf{kk}'}) \\
&+ i\left(b^\dagger_{\mathbf{k}} - b^\dagger_{\mathbf{k}'} - b_{\mathbf{k}} + b_{\mathbf{k}'}\right)\sin\phi_{\mathbf{kk}'}.
\end{aligned} \tag{24}$$

The resulting bosonic Hamiltonian after applying the HP transformations is:

$$\begin{aligned}
H_{HP} = &\sum_{\mathbf{k}} 2E_{\mathrm{UV}}\left(\frac{|\mathbf{k}|}{\mathcal{K}}\right)^m b^\dagger_{\mathbf{k}}b_{\mathbf{k}} + \sum_{\mathbf{k}\neq\mathbf{p}}\frac{V_{\mathbf{k}-\mathbf{p}}}{A}b^\dagger_{\mathbf{k}}b_{\mathbf{k}}\cos(m\phi_{\mathbf{kp}}) \\
&+ \sum_{\mathbf{k}\neq\mathbf{k}'}\frac{V_{\mathbf{k}-\mathbf{k}'}}{4A}(1 + \cos(m\phi_{\mathbf{k}_1\mathbf{k}_2}))\left(b^\dagger_{\mathbf{k}_1}b_{\mathbf{k}_2} + b_{\mathbf{k}_1}b^\dagger_{\mathbf{k}_2}\right) + \\
&+ \sum_{\mathbf{k}\neq\mathbf{k}'}\frac{V_{\mathbf{k}-\mathbf{k}'}}{4A}(1 - \cos(m\phi_{\mathbf{k}_1\mathbf{k}_2}))\left(b^\dagger_{\mathbf{k}_1}b^\dagger_{\mathbf{k}_2} + b_{\mathbf{k}_1}b_{\mathbf{k}_2}\right).
\end{aligned} \tag{25}$$

The first line contains the kinetic and self-energy terms. The second line can be viewed as boson hopping terms in the momentum lattice. The third line can be viewed as pairing terms which change the number of bosons. Lastly, by using the Bogoliubov basis given by

$$B^\dagger_{\mathbf{k}} = \begin{pmatrix} b^\dagger_{\mathbf{k}} & b_{\mathbf{k}} \end{pmatrix}, \tag{26}$$

the Hamiltonian can be expressed as

$$H_{HP} = \sum_{\mathbf{k}_1,\mathbf{k}_2} B^\dagger_{\mathbf{k}_1}H_{\mathbf{k}_1\mathbf{k}_2}B_{\mathbf{k}_2}, \tag{27}$$

with $B^\dagger_{\mathbf{k}} = \begin{pmatrix} b^\dagger_{\mathbf{k}} & b_{\mathbf{k}} \end{pmatrix}$, and

$$H_{\mathbf{k}_1\mathbf{k}_2} = \delta_{\mathbf{k}_1\mathbf{k}_2}\begin{pmatrix} 2E^m_{\mathbf{k}_1} & 0 \\ 0 & -2E^m_{\mathbf{k}_1} \end{pmatrix} - T^m_{\mathbf{k}_1\mathbf{k}_2}, \tag{28}$$

with $E_{\mathbf{k}} = v|\mathbf{k}| + \Sigma_{\mathbf{k}}$, $\Sigma_{\mathbf{k}} = \sum_{\mathbf{k}'} V_{\mathbf{k}-\mathbf{k}'}\cos(m\phi_{\mathbf{kk}'})/2A$ is the Hartree-Fock self-energy, $T_{\mathbf{kk}'}$ is

$$T_{\mathbf{kk}'} = \frac{V_{\mathbf{k}-\mathbf{k}'}}{4A}\begin{pmatrix} 1+\cos(m\phi_{\mathbf{kk}'}) & 1-\cos(m\phi_{\mathbf{kk}'}) \\ 1-\cos(m\phi_{\mathbf{kk}'}) & 1+\cos(m\phi_{\mathbf{kk}'}) \end{pmatrix}. \tag{29}$$

IV. HARTREE-FOCK SELF-ENERGY IN MULTILAYER GRAPHENE

The Hartree-Fock self-energy of the electrons and holes is given by

$$\Sigma^m(\mathbf{k}) = \int\frac{d^2\mathbf{p}}{(2\pi)^2}V(\mathbf{k}-\mathbf{p})\cos(m\phi_{\mathbf{kp}}), \tag{30}$$

The Fourier potential in (3) is then replaced in (30)

$$\Sigma^m(\mathbf{k}) = \frac{E_{\mathrm{UV}}}{\mathcal{K}^2}\int\frac{d^2\mathbf{p}}{(2\pi)^2}g_{\mathcal{K}}e^{-\frac{a^2_{\mathcal{K}}}{2}\left(\frac{\mathbf{k}-\mathbf{p}}{\mathcal{K}}\right)^2}\cos(m\phi_{\mathbf{kp}}), \tag{31}$$

In order to get an analytic expression for $\Sigma^m(\mathbf{k})$, it is defined the following integral as

$$I(k) = \int\frac{pdpd\phi}{(2\pi)^2}e^{-\left(\frac{k^2+p^2-2kp\cos\phi}{2}\right)}\cos(m\phi), \tag{32}$$

and, after substituting $x = a_{\mathcal{K}}p/\mathcal{K}$ and $y = a_{\mathcal{K}}k/\mathcal{K}$,

$$\begin{aligned}
I(k) &= \frac{\mathcal{K}^2}{a^2_{\mathcal{K}}}\int\frac{xdxd\phi}{(2\pi)^2}e^{-\left(\frac{x^2+y^2-2xy\cos\phi}{2}\right)}\cos(m\phi) \\
&= \frac{\mathcal{K}^2}{a^2_{\mathcal{K}}}\int\frac{xdx}{2\pi}e^{-\frac{x^2+y^2}{2}}\int\frac{d\phi}{2\pi}e^{xy\cos\phi}\cos(m\phi),
\end{aligned} \tag{33}$$

The polar integral is done using the Jacobi-Anger identity

$$e^{i\zeta\cos\phi} = \sum_{n=-\infty}^{+\infty}i^nJ_n(\zeta)e^{in\phi} = J_0(\zeta) + 2\sum_{n=1}^{\infty}i^nJ_n(\zeta)\cos(n\phi),$$

with imaginary argument $i\zeta = z$

$$e^{z\cos\phi} = \sum_{n=-\infty}^{+\infty}I_n(z)e^{in\phi} = J_0(z) + 2\sum_{n=1}^{\infty}I_n(z)\cos(n\phi), \tag{34}$$

so that

$$\begin{aligned}
&\int\frac{d\phi}{2\pi}e^{xy\cos(\phi)}\cos(m\phi)\\
&=\int\frac{d\phi}{2\pi}\left(I_0(xy)+2\sum_{n=1}^{\infty}I_n(xy)\cos(n\phi)\right)\cos(m\phi)\\
&=2\sum_{n=1}^{\infty}I_n(xy)\left(\int\frac{d\phi}{2\pi}\cos(n\phi)\cos(m\phi)\right)\\
&=\sum_{n=1}^{\infty}I_n(xy)\delta_{nm}=I_m(xy),
\end{aligned}\tag{35}$$

Substituting $I_m(xy)$ in the self-energy integral in Eq. (33) yields

$$\begin{aligned}
I(k)&=\frac{\mathcal{K}^2}{a_{\mathcal{K}}^2}\int\frac{xdx}{2\pi}e^{-\frac{x^2+y^2}{2}}\int\frac{d\phi}{2\pi}e^{xy\cos\phi}\cos(m\phi)\\
&=\frac{\mathcal{K}^2}{a_{\mathcal{K}}^2}\int\frac{xdx}{2\pi}e^{-\frac{x^2+y^2}{2}}I_m(xy)\\
&=\frac{\mathcal{K}^2}{a_{\mathcal{K}}^2}\frac{ye^{-\frac{y^2}{4}}}{4\sqrt{2\pi}}\left[I_{\frac{m-1}{2}}\left(\frac{y^2}{4}\right)+I_{\frac{m+1}{2}}\left(\frac{y^2}{4}\right)\right],
\end{aligned}\tag{36}$$

Finally, the self-energy of the m-layer graphene is then expressed as

$$\begin{aligned}
\Sigma^m(\mathbf{k})=&\frac{g_{\mathcal{K}}E_{\rm UV}}{8a_{\mathcal{K}}}\frac{ke^{-\frac{a_{\mathcal{K}}^2k^2}{4\mathcal{K}^2}}}{\mathcal{K}\sqrt{2\pi}}\times\\
&\times\left[I_{\frac{m-1}{2}}\left(\frac{a_{\mathcal{K}}^2k^2}{4\mathcal{K}^2}\right)+I_{\frac{m+1}{2}}\left(\frac{a_{\mathcal{K}}^2k^2}{4\mathcal{K}^2}\right)\right],
\end{aligned}\tag{37}$$

The two limit cases for large and small momenta are given by the following expressions:

$$\begin{aligned}
\lim_{k\to\infty}\Sigma^m(\mathbf{k})&=\frac{E_{\rm UV}}{4\pi a_{\mathcal{K}}^2}\\
\lim_{k\to 0}\Sigma^m(\mathbf{k})&=\frac{2^{-\frac{3n+4}{2}}E_{\rm UV}\left(\frac{a_{\mathcal{K}}k}{\mathcal{K}}\right)^n}{\sqrt{\pi}a_{\mathcal{K}}^2\Gamma\left(\frac{n+1}{2}\right)}
\end{aligned}\tag{38}$$

As special cases, the self-energy corresponding to any odd-layer and bilayer graphene are

$$\Sigma^n(\mathbf{k})=\frac{g_{\mathcal{K}}E_{\rm UV}}{8a_{\mathcal{K}}}\frac{ke^{-\frac{a_{\mathcal{K}}^2k^2}{4\mathcal{K}^2}}}{\mathcal{K}\sqrt{2\pi}}\left[I_n\left(\frac{a_{\mathcal{K}}^2k^2}{4\mathcal{K}^2}\right)+I_{n+1}\left(\frac{a_{\mathcal{K}}^2k^2}{4\mathcal{K}^2}\right)\right],\tag{39}$$

$$\begin{aligned}
\Sigma^2(\mathbf{k})=&\frac{g_{\mathcal{K}}E_{\rm UV}}{8a_{\mathcal{K}}}\frac{ke^{-\frac{a_{\mathcal{K}}^2k^2}{4\mathcal{K}^2}}}{\mathcal{K}\sqrt{2\pi}}\left[I_{\frac{1}{2}}\left(\frac{a_{\mathcal{K}}^2k^2}{4\mathcal{K}^2}\right)+I_{\frac{3}{2}}\left(\frac{a_{\mathcal{K}}^2k^2}{4\mathcal{K}^2}\right)\right]\\
=&\frac{g_{\mathcal{K}}E_{\rm UV}}{4\pi a_{\mathcal{K}}^2}\left[1-\frac{2\mathcal{K}^2}{a_{\mathcal{K}}^2k^2}\left(1-e^{-\frac{a_{\mathcal{K}}^2k^2}{2\mathcal{K}^2}}\right)\right],
\end{aligned}\tag{40}$$

where n is an odd integer (see the Fig. 3 for the cases of monolayer, bilayer and trilayer graphene). Their corresponding small-momentum regimes are described by

$$\begin{aligned}
\Sigma^1(\mathbf{k})&\approx\frac{g_{\mathcal{K}}E_{\rm UV}}{8\sqrt{2\pi}a_{\mathcal{K}}}\left(\frac{k}{\mathcal{K}}\right)+O(k^2),\\
\Sigma^2(\mathbf{k})&\approx\frac{g_{\mathcal{K}}E_{\rm UV}}{16\pi}\left(\frac{k}{\mathcal{K}}\right)^2+O(k^3),\\
\Sigma^3(\mathbf{k})&\approx\frac{a_{\mathcal{K}}E_{\rm UV}}{64\sqrt{2}\sqrt{\pi}}\left(\frac{k}{\mathcal{K}}\right)^3+O(k^4),
\end{aligned}\tag{41}$$

Notice that the dependence on $a_{\mathcal{K}}$ of the lowest-expansion-term coefficient for $\Sigma^1(\mathbf{k})$ is inverse to the dependence of $\Sigma^3(\mathbf{k})$. Even more, the lowest-expansion-term coefficient for $\Sigma^2(\mathbf{k})$ is independent of $a_{\mathcal{K}}$, as it is shown in Fig. 4.

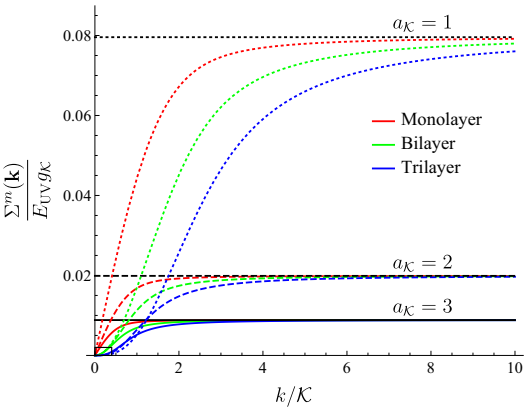

FIG. 3. Hartree-Fock self-energy $\Sigma^m(\mathbf{k})$ for monolayer ($m=1$, red), bilayer ($m=2$, green) and trilayer ($m=3$, blue) graphene. The dashing of the plots represent the value of the spreading parameter: $a_{\mathcal{K}}=1$ (dotted), $a_{\mathcal{K}}$ (dashed), and $a_{\mathcal{K}}=3$ (solid), while the horizontal black lines represent the asymptotic limit $\Sigma^m(\infty)$ the three values of $a_{\mathcal{K}}$. The little rectangle at the origin is zoomed in Fig. 4.

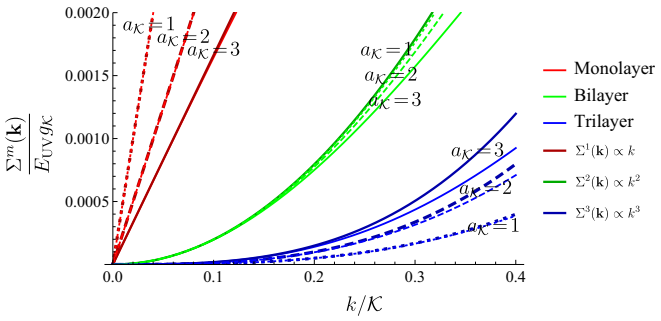

FIG. 4. Low-momentum limit for $\Sigma^m(\mathbf{k})$ in monolayer, bilayer and trilayer graphene. The legends are the same shown in Fig. 3 with the additional bolded curves representing the lowest-order expansion terms and labels of $a_{\mathcal{K}}$ to help with the interpretation of the plot. Notice that the low-momentum limit of $\Sigma^2(\mathbf{k})$ is independent of $a_{\mathcal{K}}$.

V. ANGULAR MOMENTUM CHANNELS AND PARAMETRIZATION OF THE RADIAL COORDINATE

A. General coordinate transformations on the continuum limit

We begin by taking the continuum limit of the Hamiltonian in the Bogoliubov basis (27), for this purpose it is convenient to define a rescaled Hamiltonian and boson creation operator as follows:

$$\begin{aligned} B(\mathbf{k}) &\equiv \lim_{\Delta k\to 0} \frac{B_{\mathbf{k}}}{\sqrt{\Delta k_x \Delta k_y}}, \\ H(\mathbf{k},\mathbf{k}') &\equiv \lim_{\Delta k\to 0} \frac{H_{\mathbf{k}\mathbf{k}'}}{\Delta k_x \Delta k_y}, \end{aligned} \tag{42}$$

where $\Delta k_{x,y} = 2\pi/\sqrt{A}$, A is the system area that we take to be a square. The above re-definitions allow to obtain the following continuum commutation relations for the boson operators:

$$\left[B(\mathbf{k}), B^\dagger(\mathbf{k}')\right] = \lim_{\Delta k\to 0} \mathbb{I}\frac{\delta_{\mathbf{k}\mathbf{k}'}}{(\Delta k)^2} = \mathbb{I}\delta^2(\mathbf{k}-\mathbf{k}'),$$

where

$$\mathbb{I} = \begin{pmatrix} 1 & 0 \\ 0 & -1 \end{pmatrix}. \tag{43}$$

With these rescalings we can convert the sums over momenta into continuum integrals, obtaining the continuum version of the boson Hamiltonian H_{HP} from Eq. (27):

$$\begin{aligned} \mathcal{H}_{HP} &= \lim_{\Delta k\to 0} \int \frac{d^2k}{(\Delta k)^2}\frac{d^2k'}{(\Delta k)^2} B^\dagger_{\mathbf{k}} H_{\mathbf{k}\mathbf{k}'} B_{\mathbf{k}'} \\ &= \lim_{\Delta k\to 0} (\Delta k)^4 \int \frac{d^2k}{(\Delta k)^2}\frac{d^2k'}{(\Delta k)^2} B^\dagger_\sigma(\mathbf{k}) H(\mathbf{k},\mathbf{k}') B_\sigma(\mathbf{k}') \\ &= \int d^2k d^2k' \hat{B}^\dagger_\sigma(\mathbf{k}) H(\mathbf{k},\mathbf{k}') \hat{B}_\sigma(\mathbf{k}'). \end{aligned}$$

From this continuum Hamiltonian we can perfom a change of coordinates $\mathbf{k}(\mathbf{z})$ with Jacobian $D(\mathbf{z}) = |\frac{\partial \mathbf{k}}{\partial \mathbf{z}}|$ with the following redefinitions:

$$\begin{aligned} B(\mathbf{z}) &= \sqrt{D(\mathbf{z})} B(\mathbf{k}(\mathbf{z})), \\ H(\mathbf{z},\mathbf{z}') &= \sqrt{D(\mathbf{z})D(\mathbf{z}')} H(\mathbf{k}(\mathbf{z}),\mathbf{k}(\mathbf{z}')), \end{aligned} \tag{44}$$

whose purpose is to mantain the same form of the commutation relations and the Hamiltonian as follows:

$$\begin{aligned} \left[B(\mathbf{z}), B^\dagger(\mathbf{z}')\right] &= \mathbb{I}\delta^2(\mathbf{z}-\mathbf{z}'), \\ \mathcal{H}_{HP} &= \int d^2z d^2z' \hat{B}^\dagger_\sigma(\mathbf{z}) H(\mathbf{z},\mathbf{z}') \hat{B}_\sigma(\mathbf{z}'). \end{aligned}$$

Lastly, on the new coordinate system, we proceed to re-discretize the expressions, as follows:

$$\begin{aligned} B_{\mathbf{z}} &\leftarrow \sqrt{\Delta z_1 \Delta z_2} B(\mathbf{z}), \\ H_{\mathbf{z},\mathbf{z}'} &\leftarrow \Delta z_1 \Delta z_2\, H(\mathbf{z},\mathbf{z}'), \end{aligned} \tag{45}$$

that yield the new discrete commutation relations and Hamiltonian

$$\left[B_{\mathbf{z}}, B^\dagger_{\mathbf{z}'}\right] = \mathbb{I}\delta_{\mathbf{z}\mathbf{z}'} \leftarrow \mathbb{I}\Delta k_1 \Delta k_2 \delta^2(\mathbf{z}-\mathbf{z}')$$

$$H_{HP} = \sum_{\mathbf{z},\mathbf{z}'} B^\dagger_{\mathbf{z}} H_{\mathbf{z}\mathbf{z}'} B_{\mathbf{z}'}. \tag{46}$$

Therefore, in summary, the relation between operators and the Hamiltonian matrix in the new lattice defined by the discretization of the coordinates $\mathbf{z}(\mathbf{k})$, with the original operators and Hamiltonian of the square lattice is:

$$\begin{aligned} B_{\mathbf{z}} &= \sqrt{D(\mathbf{z})\frac{\Delta z_1 \Delta z_2}{\Delta k_x \Delta k_y}} B_{\mathbf{k}} \\ H_{\mathbf{z}\mathbf{z}'} &= \sqrt{D(\mathbf{z})D(\mathbf{z}')}\frac{\Delta z_1 \Delta z_2}{\Delta k_x \Delta k_y} H_{\mathbf{k}\mathbf{k}'} \end{aligned} \tag{47}$$

The idea is that the Hamiltonian H_{HP} in Eq. (46) will produce the same physical results as the one in the square lattice in Eq. (27) of the main text in the thermodynamic limit.

B. Polar re-discretization

We choose $\mathbf{z} = (k, \phi)$ where k is the radius of the momentum vector and ϕ its polar angle. We then discretize the radial direction in two different ways specified below to check numerically that the precise form of the discretization is not crucial to the results. Therefore we choose the radial coordinate as:

$$k = k(\theta) \to k_n = k(\theta_n, \Delta\theta), \tag{48}$$

where θ is another parameter labeling the radial coordinate that we will choose to be uniformly discretized. The corresponding Jacobian for this parametrization is:

$$D(\theta) = k(\theta)\frac{dk(\theta)}{d\theta}. \tag{49}$$

The parameters θ and ϕ are uniformly discretized as follows:

$$\begin{aligned} \theta_n &= n\Delta\theta, \quad m \in \{1, \cdots, N\}, \\ \phi_l &= l\Delta\phi, \quad n \in \{-L, \cdots, L\}, \end{aligned} \tag{50}$$

FIG. 5. Depiction of the re-discretization procedure, from the initial square through the continuum limit of the system to the polar lattice and the integration of the angular coordinate in angular momentum channels reducing the dimensionality of the system to 1.

where N is the total number of slices of the radial coordinate and $2L+1$ is the total number of slices for the angular coordinate, and

$$\Delta\theta = \Delta\theta(N), \quad \Delta\phi = \frac{2\pi}{2L+1}. \tag{51}$$

The actual form of $k(\theta_n, \Delta\theta)$ is determined by the particular discretization used to calculate the matrix elements of the Hamiltonian (more details in §VI A). Therefore, the new polar lattice is determined by the sites $\mathbf{z} = (k_n, \phi_l)$ where:

$$k_n = k(n, \Delta\theta), \quad \phi_l = l\Delta\phi, \tag{52}$$

After replacing (48) and (49) into (47) we get the expression for $B_{\mathbf{k}}$ and $H_{\mathbf{k}\mathbf{k}'}$ in the polar lattice

$$\begin{aligned} B_n^l &= \frac{\mathcal{K}\sqrt{A}}{2\pi}\sqrt{\Delta\theta\Delta\phi D_n}B^\dagger_{\mathbf{k}_{nl}}, \\ H_{nn'}^{ll'} &= \frac{\mathcal{K}^2 A}{(2\pi)^2}\Delta\theta\Delta\phi\sqrt{D_n D_{n'}}H_{\mathbf{k}_{nl}\mathbf{k}_{n'l'}}, \end{aligned} \tag{53}$$

where $D_n = D(n\Delta\theta)$ and $\mathbf{k}_{nl} = \mathbf{k}(\theta_n, \phi_l)$. Finally, the whole Hamiltonian is

$$H_{HP} = \sum_{nl}\sum_{n'l'} B_n^{l\dagger} H_{nn'}^{ll'} B_{n'}^{l'}. \tag{54}$$

C. Angular momentum channels

Because the Hamiltonian matrix $H_{\mathbf{k}\mathbf{k}'}$ that enters into the Hamiltonina H_{HP} in Eq. (27) of the main text only depends on the difference between the polar angles $\phi - \phi'$ we have conservation of the angular momentum l of the bosons. Consequently, we perform Fourier transforms on the polar angles for the fields B_{mn} and the matrix $H_{mn,m'n'}$

$$\begin{aligned} B_n^l &= \frac{1}{\sqrt{2L+1}}\sum_{\ell=-L}^{L} e^{-i\ell\phi_l} B_n^\ell, \\ H_{nn'}^{ll'} &= \sum_{\ell=-L}^{L} e^{-i\ell(\phi_l - \phi_{l'})} H_{mm'}^\ell, \end{aligned} \tag{55}$$

such that the total Bogoliubov Hamiltonian decomposes into a direct sum for different angular mommentum channels, as follows:

$$H_{HP} = \sum_{nn'\ell} B_n^{\ell\dagger} H_{nn'}^\ell B_{n'}^\ell. \tag{56}$$

In that way, each dataset obtained from diagonalizing a $2N \times 2N$ matrix is labelled by the coupling constant $g_{\mathcal{K}}$ and spreading $a_{\mathcal{K}}$ of the Gaussian potential, the number of layers $m = 2$ fixed for bilayer graphene, the angular momentum ℓ and the number of sites in the radial coordinate N.

VI. NUMERICAL RESULTS

A. Description of the numerical procedure

The solution of the system is found with exact diagonalization of the $2N \times 2N$ matrix composed by the matrix elements of the Hamiltonian for the hopping ($b^\dagger_{k_1} b_{k_2}$) and pairing ($b_{k_1} b_{k_2}$, $b^\dagger_{k_1} b^\dagger_{k_2}$) terms. The parameters of the Hamiltonian are:

- Angular momentum $\ell = 0$, 1, 2, 3, 4, 5.
- Coupling constant $a_{\mathcal{K}} = 1$, 2, 5, 10.
- Reciprocal spreading $a_{\mathcal{K}} = 1$, 2, 5, 10.
- System size $N = 100$, 200, 300, 400, 500.

and the UV-cutoff being set to the unity, i.e., $\mathcal{K} = 1$ and $E_{\text{UV}} = 1$.

Regarding the spacing of the lattice for the radial component of the momentum $k_n = k(\theta_n, \Delta\theta)$, the following four parametrizations were taken into account to show that at the infinite size limit $N \to \infty$ the results do not depend on the discretization:

- Discretization by powers of n ($R = 1, 2$):

$$k_n = \mathcal{K}\left(n\Delta\theta\right)^R, \tag{57}$$

with Jacobian given by

$$D_n = \mathcal{K}^2 R\Delta k\left(n\Delta\theta\right)^{2R-1}, \tag{58}$$

and spacing

$$\Delta\theta = 1/N. \tag{59}$$

- Discretization by tangent of n ($R = 1, 2$):

$$k_n = \frac{\mathcal{K}}{\sqrt{R}}\tan^R\left(n\Delta\theta\right) \tag{60}$$

with Jacobian given by

$$D_n = \mathcal{K}^2\Delta\theta\sec^2\left(n\Delta\theta\right)\tan^{2R-1}\left(n\Delta\theta\right), \tag{61}$$

and spacing

$$\Delta\theta = \frac{\pi/2}{N+1} \tag{62}$$

Consequently, the Hamiltonians spanned by the parameter space $\{\ell, g_{\mathcal{K}}, a_{\mathcal{K}}, N, R\}$ are obtained using the parametrizations of the radial coordinate k_n, then the infinite size limit $N \to \infty$ is taken to ensure that the results are independent of the particular discretization chosen during the numerical procedures.

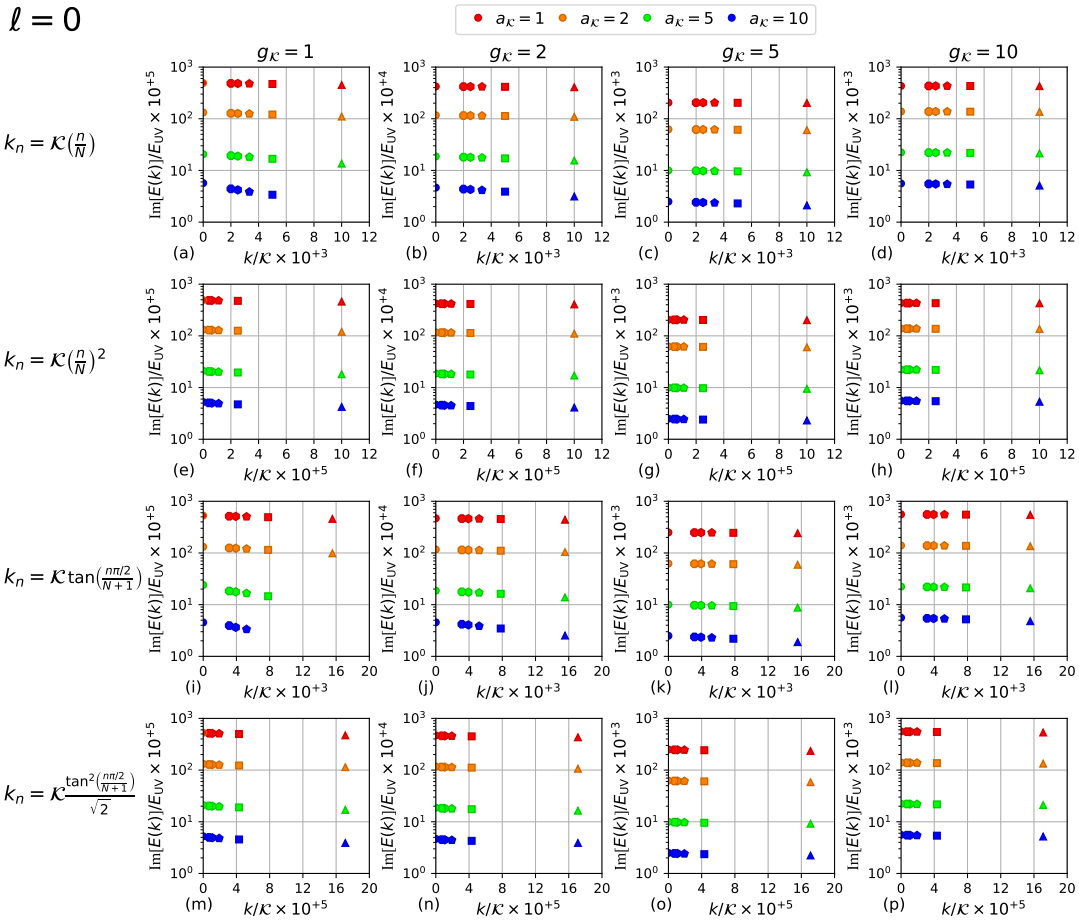

FIG. 6. Imaginary parts of the eigenvalues corresponding to the smallest momentum k_1 for $\ell = 0$ and different system sizes N: $\triangle$ ($N = 100$), $\square$ ($N = 200$), $\pentagon$ ($N = 300$), $\hexagon$ ($N = 400$), and $\bigcirc$ ($N = 500$). The extrapolation is $\bigcirc$ for $N \to \infty$.

B. Imaginary eigenvalues after doing exact diagonalization

The Hamiltonian was diagonalized for the different sets of the parameter space $\{\ell, g_\mathcal{K}, a_\mathcal{K}, N, R\}$, and then the energy spectra were examined looking for non-vanishing imaginary parts $\mathrm{Im}[E(k)]$ pointing out to an unstability in the modes of the system. The only two angular momentum channels that got non-vanishing imaginary parts in their eigenvalue spectra were $\ell = 0$ and $\ell = 2$, both showing only one eigenvalue with imaginary part (with the corresponding complementary eigenvalue with the opposite sign) at the site $n = 1$, corresponding to the smallest momentum,

$$\mathrm{Im}[E(k_{\min})] = \mathrm{Im}\left[E\left(\Delta\theta\right)\right] \neq 0, \tag{63}$$

shown in the Figs. 6 and 7 for $\ell = 0$ and $\ell = 2$, respectively. Since the imaginary eigenvalues show a finite asympthotic trend when $k_{\min} \to 0$, i.e., $N \to \infty$, the five values obtained for each system size are taken to get the infinite size limit shown as the circles $\bigcirc$ in the forementioned figures.

As expected, although the four discretizations of k_n yield different numerical results depending on the power R, the form of $k(n, \Delta k)$ (powers in Eq. (57) or tangents in Eq. (60)), or the system size N, the infinite system size limit $N \to \infty$ where $k_1 \to 0$ yields almost the same imaginary eigenvalues, with a slight increment for the tangent discretization produced by the contribution of the sites along the radial momentum beyond the UV-cutoff $\mathcal{K}$, in other words, the sites k_n with $n > N/2$.

There are some plots for small $g_\mathcal{K}$ with $R = 1$ like Fig. 6(a) or 6(c), or even worse in Fig. 7(a) and 7(c) where there are missing markers for large $a_\mathcal{K}$ that are shown in their analogues with $R = 2$, Figs. 6(b), 6(d), 7(b) and 7(d), respectively, This fact suggests that finer lattices are required to catch the non-vanishing imaginary part of the eigenvalue corresponding to the site with the smallest momentum, k_1, supporting the fact that the imaginary eigenvalue, i.e., the instalibity, is located at momentum $k \to 0$.

The main differences between $\ell = 0$ and $\ell = 2$ channels root on the relative size of their imaginary eigenvalues, being smaller for the latter channel, almost a half of those ones for the former channel. On the other hand, the

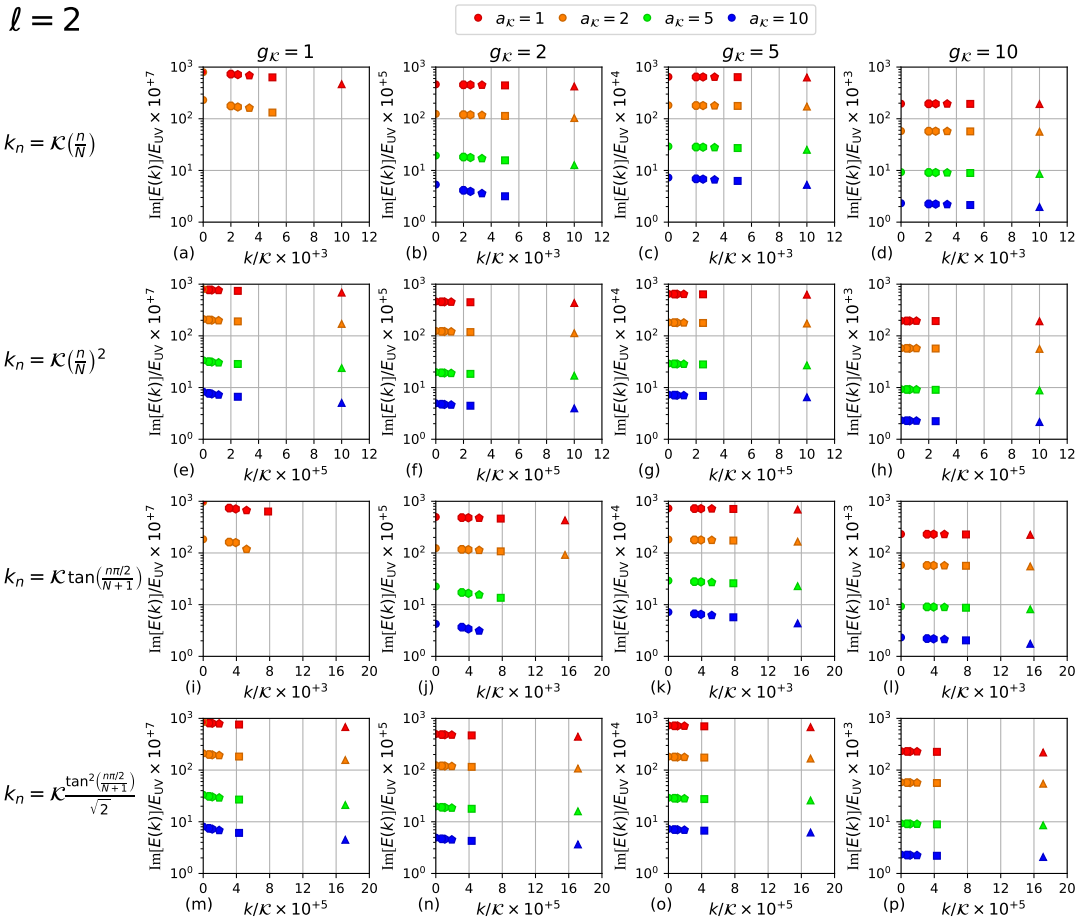

FIG. 7. Imaginary parts of the eigenvalues corresponding to the smallest momentum k_1 for $\ell = 2$ and different system sizes N: $\triangle$ ($N = 100$), $\square$ ($N = 200$), $\pentagon$ ($N = 300$), $\hexagon$ ($N = 400$), and $\bigcirc$ ($N = 500$). The extrapolation is $\bigcirc$ for $N \to \infty$.

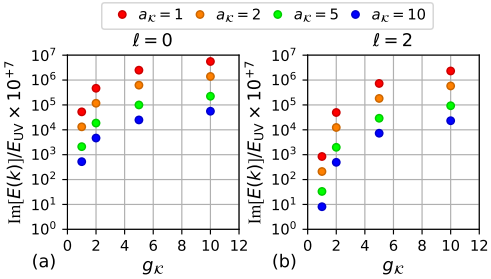

FIG. 8. Summarize of the infinite size limit $N \to \infty$ of the imaginary parts shown in Figs. 6 and 7 vs. the coupling constant $g_\mathcal{K}$.

channels show expected behaviors like the increasing of $\mathrm{Im}[E(k_{\mathrm{min}})]$ for larger $g_\mathcal{K}$, i.e., stronger interactions, and the suppression for larger $a_\mathcal{K}$, that is, a wider spreading of the potential, turning out in a weaker interaction and consequently, smaller values for $\mathrm{Im}[E(k_{\mathrm{min}})]$.

The infinite size limits for $\mathrm{Im}[E(k_{\mathrm{min}} \to 0)]$ are summarized in the Fig. 8 using the same color code and legends of Figs. 6 and 7 and the infinite size limits for the tangent discretization in Eq. (60) with $R = 2$.

VII. LOREM IPSUM

Lorem ipsum dolor sit amet, consectetur adipiscing elit. Quisque eu pharetra ligula, in scelerisque risus. Mauris convallis neque elit, at tincidunt lectus venenatis et. Donec ultricies eros nec nisl posuere, vitae scelerisque enim fringilla. Maecenas eget odio dapibus, egestas ante a, tempor neque. Nullam in nisi varius, laoreet urna sit amet, hendrerit erat. Maecenas id ligula posuere, tincidunt nisi a, scelerisque libero. Quisque maximus quis sem eleifend fermentum. Ut pharetra dui quis pharetra consectetur. Pellentesque commodo lacinia urna. Aliquam nibh nulla, facilisis id cursus eget, tristique non neque.

Proin risus sem, viverra vitae ornare ut, imperdiet a erat. Ut aliquet lorem sit amet elit efficitur auctor. Praesent consequat magna a neque feugiat, eget facilisis sem eleifend. Proin id posuere est, nec sodales nibh. Maecenas lacus felis, fringilla eu ligula at, gravida feugiat orci. In id faucibus massa. Phasellus iaculis iaculis mauris, vitae congue orci hendrerit eu. Proin interdum nisl at justo scelerisque ullamcorper. Maecenas tincidunt lectus quis gravida faucibus. Vestibulum tempor fermentum egestas.

Proin vitae semper dolor. Etiam diam ex, lobortis vitae rutrum sed, tempus at diam. Nunc ut felis mauris. Duis suscipit dui eu enim cursus, aliquet consequat est bibendum. Maecenas id enim consectetur, iaculis purus ac, consectetur quam. Suspendisse vel interdum turpis. Duis hendrerit tempor lacus, eu iaculis orci congue eu. Nam vitae tellus non nisi euismod feugiat vitae vitae ex. Quisque felis mauris, pulvinar sed dui sit amet, facilisis ultricies tortor. Quisque nibh massa, malesuada quis nisl sodales, faucibus semper ligula.

Duis imperdiet massa eu lacus fringilla, et pulvinar eros dapibus. Etiam dictum vulputate tempus. Integer felis dolor, mattis in tincidunt eu, sodales ac orci. Curabitur fermentum aliquam finibus. Praesent non dui nunc. Ut commodo vulputate lorem, nec pretium nisi lacinia vitae. Donec fermentum elementum ex vel mollis. Donec turpis nisi, placerat vel sollicitudin in, bibendum vel ipsum. Aliquam venenatis non nisl ut rutrum. Cras sed est tincidunt elit euismod fermentum et quis nisi. Ut fringilla ligula nisl, sed lobortis nunc laoreet et.

Morbi arcu leo, auctor ut luctus eu, eleifend sed lorem. Sed commodo molestie ligula ut tempor. Aenean posuere vel velit et ullamcorper. Integer consectetur semper arcu non hendrerit. Suspendisse ornare leo vel ornare sollicitudin. Vivamus elementum lacinia turpis quis suscipit. Duis varius aliquam tortor. Vestibulum ante ipsum primis in faucibus orci luctus et ultrices posuere cubilia curae; Morbi a tristique mauris. Quisque pretium, nibh in ornare elementum, neque velit efficitur dui, nec fermentum ipsum risus sit amet magna. Donec elit quam, cursus sed mollis non, aliquam vitae felis.